DALTON
FULL PAPER

# Influence of the variation of the co-ligands on the electronic transitions and emission properties of $[Pt(I)(CH_3)_3(iPr\text{-}DAB)]$, $[Pt(CH_3)_4(\alpha\text{-diimine})]$ and $[Pt(SnPh_3)_2(CH_3)_2(iPr\text{-}DAB)]$: an experimental and theoretical study

**Joris van Slageren,[a] Derk J. Stufkens,*[a] Stanislav Záliš[b] and Axel Klein[c]**

[a] *Institute of Molecular Chemistry, Universiteit van Amsterdam, Nieuwe Achtergracht 166, NL-1018 WV Amsterdam, The Netherlands*
[b] *J. Heyrovský Institute of Physical Chemistry, Czech Academy of Sciences, Dolejškova 3, CZ-18223 Praha 8, Czech Republic*
[c] *Institut für Anorganische Chemie, Universität Stuttgart, Pfaffenwaldring 55, D-70569, Stuttgart, Germany*

***Received 5th July 2001, Accepted 30th October 2001***
***First published as an Advance Article on the web 10th December 2001***

This paper reports the results of a combined spectroscopic (UV/Vis, resonance Raman, emission) and theoretical study of $[Pt(I)(CH_3)_3(iPr\text{-}DAB)]$ (iPr-DAB = *N*,*N*′-diisopropyl-1,4-diaza-1,3-butadiene), $[Pt(CH_3)_4(R\text{-}DAB)]$ (R = alkyl or aryl), $[Pt(CH_3)_4(\alpha\text{-diimine})]$ (α-diimine = pyridine-2-carbaldehyde-*N*-*tert*-butylimine or 3,4,7,8-tetramethyl-1,10-phenanthroline), and $[Pt(SnPh_3)_2(CH_3)_2(iPr\text{-}DAB)]$. The difference in character between the halide-to-ligand charge transfer (XLCT; X = I) transition of $[Pt(I)(CH_3)_3(iPr\text{-}DAB)]$ and the sigma-bond-to-ligand charge transfer (SBLCT) transitions of the other complexes, is clearly established by resonance Raman (rR) spectroscopy. DFT MO calculations confirm the assignment of the frontier orbitals and lowest-energy electronic transitions, and support the interpretation of the rR spectra. All complexes emit at low temperatures, with excited state lifetimes strongly depending on the character and reactivity of the lowest excited state.

## Introduction

The $[Pt(CH_3)_4(\alpha\text{-diimine})]$ complexes have been studied in some detail, ever since they were first reported in 1972.[1] These investigations included the reactions of these complexes with acids,[2] methyl group transfer reactions and reductive eliminations,[3] and, most importantly for this study, their photoreactivity.[4–8] This photosensitivity had already been mentioned in ref. 1, and was later shown to involve a homolytic $Pt–C_{ax}$ bond splitting reaction from a triplet excited state. This was concluded from the results of EPR,[7,8] CIDNP studies,[4,5] triplet quenching,[4,5] product analysis,[6] and, more recently, FT-EPR measurements.[9] This photoreactivity arises from the special character of the lowest-energy excited state. According to DFT MO-calculations, the LUMO consists of the lowest π* orbital of the α-diimine.[6] More remarkably, the HOMO has only a relatively small contribution from the Pt orbitals, and mainly consists of the antisymmetric combination of the axial methyl $sp^3$ orbitals. Hence, the HOMO⟶LUMO transition involves transfer of electron density from a $\sigma(C_{ax}–Pt–C_{ax})$ bonding orbital to the α-diimine ligand. This transition finally leads to $Pt–C_{ax}$ bond homolysis.

The discovery and exploration of this so-called σ⟶π* or sigma-bond-to-ligand charge transfer (SBLCT) transition,[10,11] is relatively recent. The properties of this transition and excited state have been studied in detail for several $d^6$ transition metal complexes, such as $[Re(L)(CO)_3(\alpha\text{-diimine})]$ (L = alkyl, metal fragment),[12–15] and $[M(L_1)(L_2)(CO)_2(\alpha\text{-diimine})]$ (M = Ru, Os; $L_1$, $L_2$ = *e.g.* $CH_3$, $SnPh_3$, $Mn(CO)_5$, $RuCp(CO)_2$, *etc.*).[16–20] These studies showed that if a transition metal complex contains one or more strong one-electron σ-donor ligands such as an alkyl group or metal fragment, the Re–L or $L_1–M–L_2$ (M = Ru, Os) σ-bonding orbital is often higher in energy than the metal d-orbitals. As the α-diimine ligand of the complex possesses a low-lying empty orbital, its lowest-energy transition obtains SBLCT character, since charge is transferred from the σ(Re–L) or $\sigma(L_1–M–L_2)$ orbital to the empty ligand (π*) orbital. The removal of electron density from this bonding orbital may result in photochemical Re–L or $L_1–M–L_2$ bond homolysis, with quantum yields of up to unity. However, if the metal–ligand bond is inherently strong, such as for the M–Sn complexes (M = Re, Ru, Os), this photoreaction is not very efficient, corresponding to quantum yields of only a fraction of a percent.[19] At liquid nitrogen temperature the latter complexes are completely photostable and their lowest excited states are often extremely long lived, up to 1.1 ms for $[Ru(SnPh_3)_2(CO)_2(dmb)]$ (dmb = 4,4′-dimethyl-2,2′-bipyridine).[16,19] Such excited state lifetimes are orders of magnitude larger than those of metal-to-ligand charge transfer (MLCT) excited states of structurally similar complexes, which are typically a few microseconds under these circumstances.

Closely related to the above mentioned Re, Ru, and Os complexes are the $d^6$ complexes $[Pt(L)_2(CH_3)_2(\alpha\text{-diimine})]$ in which L = $CH_3$ or $SnPh_3$. These complexes possess a similar high-lying σ(L–Pt–L) orbital and a lowest-energy SBLCT transition and corresponding excited state. In the case of $[Pt(CH_3)_4(\alpha\text{-diimine})]$ the lowest-energy transition was indeed assigned to such an SBLCT transition. However, this assignment was merely based on the results of MO-calculations,[6] and the emission properties of these complexes were barely studied. We have therefore investigated the electronic absorption, resonance Raman and emission spectra of several $[Pt(CH_3)_4(\alpha\text{-diimine})]$ (**2a**–**g**) complexes in more detail. In addition, these investigations were extended to the novel complex $[Pt(SnPh_3)_2(CH_3)_2(iPr\text{-}DAB)]$ (**3**) (iPr-DAB = *N*,*N*′-diisopropyl-1,4-diaza-1,3-butadiene) in order to establish the influence of the co-ligands on the character and properties of the lowest excited state and to compare its excited state properties with those of the

 DOI: 10.1039/b105979n

isoelectronic complexes $[M(SnPh_3)_2(CO)_2(iPr\text{-}DAB)]$ (M = Ru, Os). Further variation of the co-ligands was achieved by studying the lowest-energy transition and excited state of the complex $[Pt(I)(CH_3)_3(iPr\text{-}DAB)]$ (**1**). Resonance Raman spectroscopy was used for these investigations since it is one of the few experimental techniques that can characterise allowed electronic transitions giving rise to absorption bands. In addition, DFT MO calculations were performed to determine the character of the molecular orbitals and to assign the electronic transitions, in conjunction with the vibrations observed in the resonance Raman spectra. The α-diimine ligand in the complexes $[Pt(CH_3)_4(\alpha\text{-diimine})]$ was varied in order to establish the electronic and steric effects of such ligands on the excited state. For instance, the ligand tmphen (3,4,7,8-tetramethyl-1,10-phenanthroline) is known to provide highly luminescent complexes with rather long excited-state lifetimes, because of its rigidity and high-lying lowest π* level. In this respect, the complexes of tBu-Pyca (pyridine-2-carbaldehyde-*tert*-butylimine) are normally intermediate in their behaviour between the aliphatic DAB ligands and aromatic α-diimine ligands such as 2,2′-bipyridine or 1,10-phenanthroline.[6]

Fig. 1 presents the general structure of the complexes under

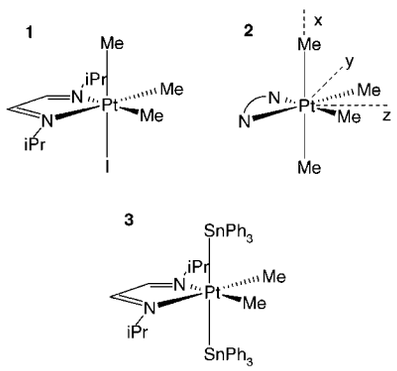


**Fig. 1** Schematic structures of the complexes under study.

study. It is shown that variation of the axial ligands going from **1** to **2** to **3** has a dramatic effect on the spectroscopic and excited state properties.

## Experimental

### Materials

$I_2$ (Merck), $SnClPh_3$ (Merck, zur Synthese), tmphen (3,4,7,8-tetramethyl-1,10-phenanthroline, Aldrich, 99+%) were used as received. NaK alloy was prepared by carefully heating freshly etched sodium (1 part) and potassium (3 parts) in toluene under nitrogen. Solvents purchased from Acros (THF, hexane, dichloromethane, acetonitrile, 2-MeTHF) were dried over and distilled from the appropriate drying agent when necessary. Silica gel (kieselgel 60, Merck, 70–230 mesh) for column chromatography was dried and activated by heating *in vacuo* at 160 °C overnight.

### Syntheses

All syntheses were performed under a nitrogen atmosphere using standard Schlenk techniques. The complexes $[Pt(CH_3)_4(R\text{-}DAB)]$ (**2a**–**e**),[8] $[Pt(CH_3)_4(tBu\text{-}Pyca)]$ (tBu-Pyca = pyridine-2-carbaldehyde-*N*-*tert*-butylimine) (**2f**),[8] $[Pt(CH_3)_2(iPr\text{-}DAB)]$,[8] as well as *N*,*N*′-diisopropyl-1,4-diazabutadiene (iPr-DAB),[21] were prepared according to literature procedures.

**$[Pt(I)_2(CH_3)_2(iPr\text{-}DAB)]$.** An excess of $I_2$ was added to a solution of $[Pt(CH_3)_2(iPr\text{-}DAB)]$ in $CH_2Cl_2$. Evaporation of the solvent and subsequent washing with pentane yielded the product as a dark brown powder in 60% yield. $^1$H NMR ($CDCl_3$); $\delta$: 1.55 (d, $^3J$ = 6.6 Hz, 12H, $CH(CH_3)_2$); 2.24 (s, $J_{Pt-H}$ = 73.1 Hz, 6H, Pt–$CH_3$); 4.63 (septet, $^3J$ = 6.6 Hz, 2H, $CH(CH_3)_2$); 8.53 (s, $J_{Pt-H}$ = 30.9 Hz, 2H, imine H).

**$[Pt(I)(CH_3)_3(iPr\text{-}DAB)]$ (1).** Was prepared by oxidative addition of $CH_3I$ to $[Pt(CH_3)_2(iPr\text{-}DAB)]$ in near-quantitative yield.[22,23] UV-Vis (THF); $\lambda_{max}$($\varepsilon$ in $M^{-1}$ $cm^{-1}$): 263 (6725), 406 (635) nm. $^1$H NMR ($CDCl_3$); $\delta$: 0.66 (s, $J_{Pt-H}$ = 72.6 Hz, 3H, Pt–$Me_{ax}$); 1.42 (s, $J_{Pt-H}$ = 70.2 Hz, 6H, Pt–$Me_{eq}$); 1.41 (d, $^3J$ = 6.6 Hz, 6H, iPr-DAB $CH_3$); 1.54 (d, $^3J$ = 6.6 Hz, 6H, $CH(CH_3)_2$); 4.64 (septet, $^3J$ = 6.6 Hz, 2H, $CH(CH_3)_2$), 8.61 (s, $J_{Pt-H}$ = 28.2 Hz, 2H, imine H).

**$[Pt(CD_3)_4(iPr\text{-}DAB)]$ (2b).** Was prepared from $CD_3Li$, $CD_3I$ and $[Pt(Cl)_2(SMe_2)_2]$ according to the same procedure as for $[Pt(CH_3)_4(R\text{-}DAB)]$.[8] Yield 60%. $^1$H NMR ($CD_2Cl_2$); $\delta$: 1.35 (d, $^3J$ = 6.6 Hz, 12H, $CH(CH_3)_2$); 4.56 (septet, $^3J$ = 6.6 Hz, 2H, $CH(CH_3)_2$), 8.63 (s, $J_{Pt-H}$ = 31.5 Hz, 2H, imine H).

**$[Pt(CH_3)_4(tmphen)]$ (2g).** Was prepared according to the same procedure as $[Pt(CH_3)_4(R\text{-}DAB)]$.[8] Yield 88%. Anal. Calcd. for $C_{20}H_{28}N_2Pt$: C, 48.87; H, 5.74; N, 5.70. Found: C, 48.91; H, 5.77; N, 5.72%. $^1$H NMR ($C_6D_6$): $\delta$: 0.39 (s, $J_{Pt-H}$ = 44 Hz, 3H, Pt–$Me_{ax}$); 1.97 (s, $J_{Pt-H}$ = 72.6 Hz, 6H, Pt–$Me_{eq}$); 1.69 (s, 6H, tmphen 4,7-$CH_3$); 1.89 (s, 6H, tmphen 3,8-$CH_3$); 7.41 (s, 2H, tmphen H 5,6); 9.01 (s, $J_{Pt-H}$ = 15.3 Hz, 2H, tmphen H 2,9).

**$[Pt(SnPh_3)_2(CH_3)_2(iPr\text{-}DAB)]$ (3).** A setup consisting of two two-necked Schlenk vessels connected by a G3 glass frit, was assembled. Water was rigorously removed by heating under vacuum. One Schlenk vessel was charged with 106 mg $[Pt(I)_2(CH_3)_2(iPr\text{-}DAB)]$ and the other with a solution of 162 mg $SnClPh_3$ in THF. The latter solution was freeze–pump–thaw degassed three times, after which THF was added to the platinum compound. After addition of an excess of NaK alloy to the brownish solution of $[Pt(I)_2(CH_3)_2(iPr\text{-}DAB)]$, the solution turned purple and later brown-yellow. This extremely air-sensitive intermediate was filtered over a G3 glass filter into the solution of $SnClPh_3$, which turned blue-green immediately. Evaporation of the solvent yielded a green solid, which was purified using column chromatography (activated silica, $CH_2Cl_2$/hexane gradient elution). The desired blue complex eluted in the first fraction and was obtained in a low percentage yield. The second fraction contained a brown-red compound of unclear composition. FAB-MS; *m*/*z*: ($M^+$ not detected), 716.16 ($M^+ - SnPh_3$). UV-Vis (THF); $\lambda_{max}$($\varepsilon$ in $M^{-1}$ $cm^{-1}$): 281 (5233), 350 (17404), 640 (1056) nm. $^1$H NMR ($CD_2Cl_2$); $\delta$: 0.94 (d, $^3J$ = 6.6 Hz, 12H, $CH(CH_3)_2$), 1.34 (s, $J_{Pt-H}$ = 67.8 Hz, $J_{Sn-H}$ = 23.4 Hz, 6H, Pt–$CH_3$) 4.67 (sept, $^3J$ = 6.6 Hz, 2H, $CH(CH_3)_2$), 7.25 (m, 9H, *m*/*p*-$SnC_6H_5$), 7.29 (m, 6H, *o*-$SnC_6H_5$), 8.44 (m, $J_{Sn-H}$, $J_{Pt-H}$ = 29.1 Hz, 37.2 Hz, 2H, imine H). $^{13}$C NMR APT ($CD_2Cl_2$); $\delta$: −19.1 (s, Pt–$CH_3$), 25.8 (s, $CH(CH_3)_2$), 68.0 (s, $CH(CH_3)_2$), 129.4 (s, $J_{Sn-C}$ = 62 Hz, *m*-$SnC_6H_5$), 130.7 (s, *p*-$SnC_6H_5$), 136.3 (s, $J_{Sn-C}$ = 50 Hz, *o*-$SnC_6H_5$), 137.5 (s, $J_{Sn-C}$ = 15 Hz, imine C), 138.1 (s, *ipso*-$SnC_6H_5$).

### Spectroscopic measurements

All spectroscopic measurements were performed under a nitrogen atmosphere. Electronic absorption spectra on Varian Cary 4E and Hewlett-Packard 8453 spectrophotometers. NMR spectra were recorded on a Varian Mercury 300 (300.13 MHz and 75.46 MHz for $^1$H and $^{13}$C, respectively) spectrometer. Resonance Raman spectra of the complexes dispersed in $KNO_3$ pellets or in dichloromethane solution were recorded on a Dilor XY spectrometer equipped with a Wright Instruments CCD detector, using a Spectra Physics 2040E $Ar^+$ laser in combination with Coherent CR490 and CR590 dye lasers (with Coumarin 6 and Rhodamine 6G dyes) as the excitation sources. Nanosecond time-resolved electronic absorption and emission spectra were obtained with Spectra Physics GCR3 Nd : YAG and Coherent Infinity XPO excitation sources and an OMA detection system, described previously.[24]

### Computational details

The calculations concerned the orbital and singlet excitation energies of the complexes under study as well as the frequency and character of their vibrations observed in the resonance Raman spectra. The $SnPh_3$ moiety was replaced by $SnH_3$ in all calculations. The ground state electronic structures of $[Pt(I)(CH_3)_3(iPr\text{-}DAB)]$ (**1**), $[Pt(CH_3)_4(iPr\text{-}DAB)]$ (**2a**) and $[Pt(SnH_3)_2(CH_3)_2(iPr\text{-}DAB)]$ (**3***, a model complex for **3**) were calculated by density functional theory (DFT) methods using the ADF1999[24,25] programme package, while Gaussian 98[26] was used for the calculations of the vibrations. The lowest-energy electronic transitions of the closed shell complexes were calculated by time-dependent DFT methods using the ADF-RESPONSE[27] and G98 programmes.

Within Gaussian 98, Dunning's polarized valence double ζ basis sets[28] were used for C, N and H atoms and the effective quasirelativistic effective core pseudopotentials and corresponding optimized set of basis functions[29,30] for Pt, I and Sn. In these calculations, the hybrid Becke's three parameter functional with the Lee, Yang and Parr correlation functional (B3LYP)[31] were used.

Within the ADF program, Slater type orbital (STO) basis sets of triple ζ quality with polarisation functions for Pt and double ζ with polarisation functions for remaining atoms were employed. The inner shells were represented by a frozen core approximation, *viz*. 1s for C, N, 1s–3d for I, 1s–4d for Pt and 1s–4p for Sn were kept frozen. The following density functionals were used within ADF: a local density approximation (LDA) with VWN parametrisation of electron gas data or a functional including Becke's gradient correction[32] to the local exchange expression in conjunction with Perdew's gradient correction[33] to the LDA expression (BP). The scalar relativistic (SR) zero order regular approximation (ZORA) was used within this study. The adiabatic local density approximation (ALDA), ignoring the frequency dependence, was used in post-SCF time-dependent DFT calculations.[27]

The calculations on $[Pt(CH_3)_4(R\text{-}DAB)]$ and $[Pt(SnH_3)_2(CH_3)_2(R\text{-}DAB)]$ were performed in constrained $C_{2v}$ symmetry, with the *z*-axis coincident with the $C_2$ symmetry axis. The R-DAB ligand and the C atoms of the equatorial $CH_3$ groups are located in the *yz* plane and the $SnH_3/CH_3$ axial ligands lie on the *x* axis. Calculations on $[Pt(I)(CH_3)_3(R\text{-}DAB)]$ (**1**) were performed in constrained $C_s$ symmetry, with the *z*-axis bisecting the DAB ligand as above.

## Results and discussion

### Synthesis

Fig. 1 shows the compounds under study. The syntheses of $[Pt(I)(CH_3)_3(iPr\text{-}DAB)]$ (**1**) and$[Pt(CH_3)_4(\alpha\text{-diimine})]$ (**2a**–**g**) are fairly straightforward and proceed according to literature methods.[8,22,23] The synthesis of $[Pt(SnPh_3)_2(CH_3)_2(iPr\text{-}DAB)]$ (**3**), on the other hand, is not straightforward. Attempts to react $[Pt(I)_2(CH_3)_2(iPr\text{-}DAB)]$ with $LiSnPh_3$ resulted in decomposition. Instead $[Pt(I)_2(CH_3)_2(iPr\text{-}DAB)]$ was reduced using NaK alloy to yield a highly reactive intermediate, which was allowed to react with two equivalents of $SnClPh_3$. This synthetic strategy has been successfully employed in the case of $[Os(SnPh_3)_2(CO)_2(iPr\text{-}DAB)]$.[19] In the first step of this synthesis, the initially brownish solution of $[Pt(I)_2(CH_3)_2(iPr\text{-}DAB)]$ in THF turned purple and after about one hour brown-yellow. The final solution was extremely air sensitive, and turned purple upon exposure to (traces of) oxygen, presumably due to reoxidation to the intermediate of the reduction. Because of this sensitivity the solution of $ClSnPh_3$ in THF (despite the solvent being routinely distilled over Na/benzophenone under nitrogen) had to be degassed. Otherwise, the $ClSnPh_3$ solution turned purple immediately upon addition of the solution containing the reduction product of $[Pt(I)_2(CH_3)_2(iPr\text{-}DAB)]$. Column chromatography over activated silica was necessary for the purification of **3**. However, since **3** is rather unstable on the chromatography column, fairly low yields were obtained (in the order of a few percent). The $FAB^+$-MS spectrum did not show the molecular ion, which is rather uncommon for this series of complexes.[19,34,35] However, the isotope pattern around the peak observed at *m*/*z* 716.16, corresponded exactly to that calculated for $C_{28}H_{37}N_2SnPt$ or $[Pt(SnPh_3)(CH_3)_2(iPr\text{-}DAB)]^+$.

The proton and carbon NMR spectra showed that the methyl groups of the iPr-DAB ligand, which point in the direction of the axial ligands, have the same chemical shift. The chemical shift of these protons is very sensitive to the nature of these ligands. For example, they were found to be different in complexes such as $[Ru(SnPh_3)(CO)_2(iPr\text{-}DAB)]_2$ and $[Ru(SnPh_3)(SnMe_3)(CO)_2(iPr\text{-}DAB)]$.[34,36] Therefore, the two axial ligands must be the same in this complex. The resonance due to the methyl groups bound to the Pt atom was found at $\delta$ 1.34, which is much closer to the $\delta$ 1.42 found for the equatorial methyl group in $[Pt(I)(CH_3)_3(iPr\text{-}DAB)]$ (**1**) rather than the $\delta$ 0.66 found for the axial one. From this we conclude that the methyl groups of **3** are located in the equatorial plane and that this complex has the structure shown in Fig. 1 and should be formulated as *trans*, *cis*-$[Pt(SnPh_3)_2(CH_3)_2(iPr\text{-}DAB)]$. Although several other organometallic Pt(IV) complexes with a Pt–Sn bond are known,[37–40] only a few compounds with a trinuclear Sn–Pt–Sn bonded system have been reported.[41,42]

### Absorption spectra and MO calculations

Complexes **2** and **3** absorb in the visible region, whereas **1** absorbs only at higher energy (Table 1, Fig. 2). The assignments

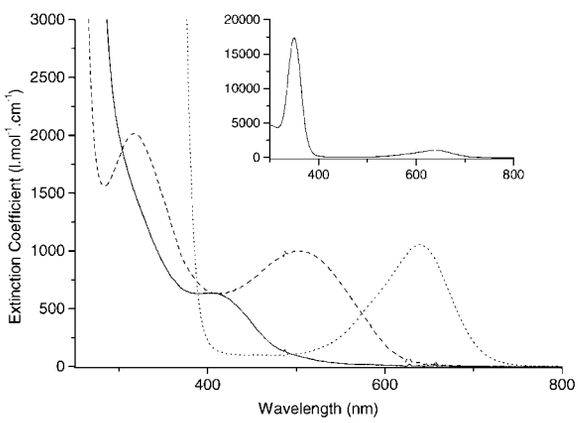


**Fig. 2** UV/Vis absorption spectra of $[Pt(I)(CH_3)_3(iPr\text{-}DAB)]$ (**1**, —), $[Pt(CH_3)_4(iPr\text{-}DAB)]$ (**2a**, - - -) and $[Pt(SnPh_3)_2(CH_3)_2(iPr\text{-}DAB)]$ (**3**, · · ·) in THF at room temperature. The inset shows the complete spectrum of **3**.

of the lowest-energy absorption bands are based in part on DFT MO-calculations on complexes **1**, **2a** and $[Pt(SnH_3)_2(CH_3)_2(iPr\text{-}DAB)]$ (**3***), the latter complex serving as a model compound for **3**. The character of the electronic transitions was further clarified by the resonance Raman (rR) spectra, obtained by excitation into the lowest-energy absorption band. The results of the calculations are collected in Tables 2–6, the rR spectra will be discussed in the next section.

Complex **1** shows two absorption bands in the UV region of the spectrum, namely at 263 and 406 nm (in THF) with molar absorptivities of 6725 and 635 $M^{-1}$ $cm^{-1}$, respectively. The highest occupied MOs of complex **1** are clearly different in character from those of the other complexes. They consist of a set of almost degenerate orbitals (27a″ and 37a′) both having $p_\pi$ (I) character (Table 2). The lower-lying occupied orbital 36a′ is a σ(I–Pt–$CH_3$) orbital, again mainly halide in character, while below this MO there is a set of metal localized MOs (not shown). The LUMO (38a′) has mainly (86%) π*(iPr-DAB) character. The two lowest-energy symmetry allowed (a′⟶a′)

**Table 1** Long-wavelength absorption maxima

| | Compound | $\lambda_{max}$ (toluene)/nm | $\lambda_{max}$ (MeCN)/nm | $\Delta$/cm$^{-1}$ [a] |
|---|---|---|---|---|
| **1** | $[Pt(I)(CH_3)_3(iPr\text{-}DAB)]$ | 432 | 372 | 3734 |
| **2a** | $[Pt(CH_3)_4(iPr\text{-}DAB)]$ | 531 | 479 | 2044 |
| **2b** | $[Pt(CD_3)_4(iPr\text{-}DAB)]$ | 515 | 464 | 2134 |
| **2c** | $[Pt(CH_3)_4(tBu\text{-}DAB)]$ [b] | 520 | 471 | 2001 |
| **2d** | $[Pt(CH_3)_4(cHx\text{-}DAB)]$ [b] | 532 | 485 | 1822 |
| **2e** | $[Pt(CH_3)_4(Xyl\text{-}DAB)]$ [b] | 605 | 550 | 1653 |
| **2f** | $[Pt(CH_3)_4(tBu\text{-}Pyca)]$ [b] | 493 | 449 | 1988 |
| **2g** | $[Pt(CH_3)_4(tmphen)]$ | 446 | 410 | 1969 |
| **3** | $[Pt(SnPh_3)_2(CH_3)_2(iPr\text{-}DAB)]$ | 657 | 620 | 908 |

[a] $\nu$(MeCN)–$\nu$(toluene). [b] From ref. 6.

**Table 2** ADF calculated one-electron energies and percentage composition of selected highest-occupied and lowest-unoccupied molecular orbitals of $[Pt(I)(CH_3)_3(iPr\text{-}DAB)]$ (**1**) expressed in terms of compositional fragments

| MO | E/eV | Prevailing character | Pt | I | $Me_{ax}$ | $Me_{eq}$ | iPr-DAB |
|---|---|---|---|---|---|---|---|
| Unoccupied | | | | | | | |
| 38a′ | −3.84 | π* R-DAB | 7 ($d_{xy}$); 1 ($p_x$) | 6 | 1 | | 86 (π*) |
| Occupied | | | | | | | |
| 27a″ | −4.75 | I($p_\pi$) + Pt($d_\pi$) | 6 ($d_{xz}$) | 91 | | 1 | 1 |
| 37a′ | −4.78 | I($p_\pi$) + Pt($d_\pi$) | 3 ($d_{xy}$) | 94 | | 1 | 1 |
| 36a′ | −5.57 | I(σ), Pt, Me(σ) | 7 ($p_x$); 1 ($d_{z^2}$); 4 ($d_{xy}$) | 59 | 20 | 5 | 3 |

**Table 3** ADF calculated one-electron energies and percentage composition of selected highest-occupied and lowest-unoccupied molecular orbitals of $[Pt(CH_3)_4(iPr\text{-}DAB)]$ (**2a**) expressed in terms of compositional fragments

| MO | *E*/eV | Prevailing character | Pt | $(Me)_{ax}$ | $(Me)_{eq}$ | iPr-DAB |
|---|---|---|---|---|---|---|
| Unoccupied | | | | | | |
| $14b_1$ | −3.35 | π* R-DAB + $(Me)_{ax}$ | 8 ($d_{xz}$); 1 ($p_x$) | 14 | | 77 (π*) |
| Occupied | | | | | | |
| $13b_1$ | −4.79 | $Me_{ax}$ + Pt + π* R-DAB | 9 ($p_x$); 1 ($d_{xz}$) | 73 | 3 | 13 |
| $9a_2$ | −5.48 | $d_{Pt}$ + π* R-DAB | 75 ($d_{xy}$); | 8 | 4 | 12 |
| $21a_1$ | −5.71 | $d_{Pt}$ + $Me_{eq}$ | 53 ($d_{z^2}$); 22 ($d_{x^2-y^2}$) | | 17 | 7 |
| $12b_1$ | −5.93 | $d_{Pt}$ + R-DAB | 71 ($d_{xz}$); 1 ($p_x$) | 10 | 6 | 12 |

**Table 4** TD DFT calculated lowest-energy singlet excitation energies and observed absorption maxima of $[Pt(CH_3)_4(iPr\text{-}DAB)]$ (**2a**)

| | | Calculated transition | | | |
|---|---|---|---|---|---|
| State | Composition | /eV | /nm | $\lambda_{abs}$/nm [a] | Calc. osc. strength |
| $^1A_1$ | 93% ($13b_1 \longrightarrow 14b_1$) | 1.99 | 623 | 531 | 0.021 |
| $^1B_2$ | 94% ($9a_2 \longrightarrow 14b_1$) | 2.26 | 549 | n.o. [b] | 0.002 |
| $^1A_1$ | 91% ($12b_1 \longrightarrow 14b_1$) | 3.21 | 386 | 326 | 0.072 |

[a] Observed wavelength maximum in toluene at room temperature. [b] Not observed.

**Table 5** ADF calculated one-electron energies and percentage composition of selected highest-occupied and lowest-unoccupied molecular orbitals of $[Pt(SnH_3)_2(CH_3)_2(iPr\text{-}DAB)]$ (**3***) expressed in terms of compositional fragments

| MO | *E*/eV | Prevailing character | Pt | $SnH_3$ | Me | iPr-DAB |
|---|---|---|---|---|---|---|
| Unoccupied | | | | | | |
| $25a_1$ | −1.41 | $d_{Pt}$ + $SnH_3$ | 6 ($d_{z^2}$); 13 ($d_{x^2-y^2}$) | 70 | 7 | 4 |
| $17b_1$ | −3.54 | π* R-DAB + $SnH_3$ | 5($d_{xz}$); 1 ($p_x$) | 23 | | 71(π*) |
| Occupied | | | | | | |
| $16b_1$ | −4.87 | $SnH_3$ + Pt + π* R-DAB | 10 ($p_x$); 6 ($d_{xz}$) | 60 | 5 | 18 |
| $11a_2$ | −6.18 | $d_{Pt}$ + π* R-DAB | 67 ($d_{xy}$) | 5 | 6 | 22 |
| $24a_1$ | −6.21 | $d_{Pt}$ + Me | 50 ($d_{z^2}$); 23 ($d_{x^2-y^2}$) | | 18 | 8 |
| $18b_2$ | −6.57 | π R-DAB + $d_{Pt}$ + Me | 12 ($d_{yz}$); 3 ($p_y$) | 6 | 38 | 41 |
| $15b_1$ | −6.64 | $d_{Pt}$ + R-DAB | 66 ($d_{xz}$); 1 ($p_x$) | 13 | 6 | 14 |
| $14b_1$ | −7.27 | $SnH_3$ | 4 ($d_{xz}$) | 84 | 6 | 6 |
| $22a_1$ | −7.43 | $SnH_3$ | 2 (s); 1 ($d_{z^2}$) | 87 | 7 | 2 |

transitions are therefore expected to have halide-to-ligand charge transfer (XLCT, X = I) character. This expectation is supported by time-dependent (TD) DFT calculations which show that these transitions have 98% 37a′⟶38a′ and 98% 36a′⟶38a′ character, respectively. The ADF/BP calculated (vacuum) energies of the lowest-energy transitions (0.98 eV and 1.94 eV) are much lower than the observed lowest-energy absorption maxima in solution (2.87 and ≈3.87 eV in toluene). This difference is too large to be caused by the difference in medium between theory and experiment. The G98/B3LYP

**Table 6** TD DFT calculated lowest-energy singlet excitation energies (eV) of the model complex $[Pt(SnH_3)_2(CH_3)_2(iPr\text{-}DAB)]$ (**3***)

| State | Composition | Calculated transition /eV | /nm | $\lambda_{abs}$/nm[a] | Calc. osc. strength |
|---|---|---|---|---|---|
| $^1A_1$ | 96% ($16b_1 \longrightarrow 17b_1$) | 1.89 | 656 | 657 | 0.028 |
| $^1B_2$ | 94% ($11a_2 \longrightarrow 17b_1$) | 2.80 | 443 | n.o.[b] | 0.007 |
| $^1A_1$ | 86% ($15b_1 \longrightarrow 17b_1$); 10% ($14b_1 \longrightarrow 17b_1$) | 3.49 | 355 | n.o.[b] | 0.029 |
| $^1B_1$ | 68% ($16b_1 \longrightarrow 25a_1$); 20% ($22a_1 \longrightarrow 17b_1$) | 3.85 | 322 | 351 | 0.248 |
| $^1A_1$ | 89% ($14b_1 \longrightarrow 17b_1$) | 3.88 | 320 | n.o.[b] | 0.028 |
| $^1B_1$ | 79% ($22a_1 \longrightarrow 17b_1$); 14% ($16b_1 \longrightarrow 25a_1$) | 3.98 | 311 | n.o.[b] | 0.078 |

[a] Observed absorption maximum for $[Pt(SnPh_3)_2(CH_3)_2(iPr\text{-}DAB)]$ in toluene at room temperature. [b] Not observed.

calculated values of 1.78 eV and 2.48 eV are closer to the experimental ones, but still too low. Such a discrepancy is not uncommon for DFT calculations on transition metal complexes possessing metal–halide bonds.[43–45]

Complexes **2** have one absorption band in the visible region at wavelengths varying from 446 nm (**2g** in toluene) to 605 nm (**2e** in toluene) in accordance with the energy of the lowest π* orbital of the α-diimine ligand, which is relatively high in the case of **2g** (tmphen) and rather low for **2e** (Xyl-DAB). These absorption bands have molar absorptivities around 1000 $M^{-1}$ $cm^{-1}$ (see Fig. 2 and ref. 6) and are quite solvatochromic; they shift by about 2000 $cm^{-1}$ bathochromically going from acetonitrile to the less polar toluene. All complexes have a second absorption band at 300–350 nm which is about twice as intense. The lowest-energy absorption bands are assigned with the help of DFT MO-calculations on $[Pt(CH_3)_4(iPr\text{-}DAB)]$ (**2a**) which are in line with those of earlier calculations on the $[Pt(CH_3)_4(H\text{-}DAB)]$ model complex.[6] Thus, the HOMO is mainly composed of the antisymmetric combination of the axial $sp^3(CH_3)$ orbitals and $p_x(Pt)$, while the LUMO mainly consists of the lowest π* orbital of the iPr-DAB ligand (see Fig. 1 for the orientation of the axes). According to our DFT calculations (Table 3), some mixing between the σ and π* orbitals occurs in both the HOMO and the LUMO. The lowest-energy transition has 93% $13b_1 \longrightarrow 14b_1$ (HOMO⟶LUMO) character according to TD DFT calculations (Table 4). In view of the characters of the orbitals involved, it can best be described as a sigma-bond-to-ligand charge transfer (SBLCT) transition. The second allowed transition (91% $12b_1 \longrightarrow 14b_1$) has MLCT character. The absorption maxima, calculated under vacuum, are at lower energies (623 and 386 nm, respectively, Table 4) than observed (531 and 326 nm in toluene, respectively), which is not unexpected in view of the solvent dependence of the experimental values.

Complex **3** has its lowest-energy absorption band at 640 nm (THF) with a molar absorptivity of 1056 $M^{-1}$ $cm^{-1}$. Other bands are found at 281 and 350 nm (THF) with molar absorptivities of 5233 and 17404 $M^{-1}cm^{-1}$, respectively. Again the characters of the lowest-energy absorption bands are assigned with the use of DFT MO-calculations. The character of the relevant MOs and calculated electronic transitions of $[Pt(SnH_3)_2(CH_3)_2(iPr\text{-}DAB)]$ (**3***, a model complex for **3**) are similar to those of **2a**. A slightly stronger σ–π* mixing is present in the frontier orbitals (Table 5) of **3***. Thus, the contribution of the lowest π*(iPr-DAB) orbital to the HOMO is 18%, compared to 13% in the case of **2a**. Similarly, the contribution of the axial ligands to the LUMO is 23% in the case of $[Pt(SnH_3)_2(CH_3)_2(iPr\text{-}DAB)]$, but only 14% for **2a**. On the other hand, the σ–π* interaction in $[Pt(SnH_3)_2(CH_3)_2(iPr\text{-}DAB)]$ is still significantly weaker than in the closely related model complex $[Ru(SnH_3)_2(CO)_2(H\text{-}DAB)]$.[17] In this latter complex the contributions of π*(iPr-DAB) to the HOMO and of $SnH_3$ to the LUMO are both 27%, according to DFT calculations. Recent calculations on $[Ru(SnH_3)_2(CO)_2(iPr\text{-}DAB)]$ showed that this difference is certainly not due to replacement of iPr-DAB by H-DAB in the former calculations.[46] The stronger σ–π* interaction in the Ru- and Os-complexes causes a stabilisation of their HOMO with respect to that of **3*** and is also responsible for the shift of the first absorption band to higher energy, going from **3** (657 nm in toluene) to $[M(SnPh_3)_2(CO)_2(iPr\text{-}DAB)]$ (M = Ru, Os) (523 and 497 nm in toluene, respectively).[17,19] Another consequence of the weaker σ–π* interaction for **3** is a lowering of the molar absorptivity from over 6000 $M^{-1}cm^{-1}$ in the case of the Ru/Os complexes to 1056 $M^{-1}cm^{-1}$ for **3**, which is in fact very similar to the molar absorptivities of complexes **2**.

The calculated energy of the first allowed electronic transition of **3*** (655 nm, Table 6) is the same as observed for **3** (657 nm in toluene). The second absorption band (observed at 351 nm in toluene for **3**) seems to consist of three allowed transitions (Table 6) of very mixed character. The observed ratio of the molar absorptivities for the low and high energy absorptions (1 : 10) (Fig. 2), fits very well with that of the calculated oscillator strengths for the corresponding transitions of **3***.

### Resonance Raman spectra

In order to further characterize the electronic transitions and confirm their assignment, the resonance Raman (rR) spectra of the complexes **1**, **2a**–**g** and **3** were investigated. Such spectra, obtained by excitation into an allowed electronic transition, show resonance enhancement of the Raman intensity for those vibrations which are most strongly affected by that particular electronic transition.[47] Hence by learning which vibrations are most strongly affected by a specific electronic transition, valuable information can be obtained about its character. The complexes containing aliphatic R-DAB ligands are especially suited for this study, since the simple structure of these ligands simplifies the rR spectra of their complexes. In order to assist in the assignment of the Raman bands, the relevant vibrational frequencies of $[Pt(I)(CH_3)_3(iPr\text{-}DAB)]$ (**1**), $[Pt(CH_3)_4(iPr\text{-}DAB)]$ (**2a**), $[Pt(CD_3)_4(iPr\text{-}DAB)]$ (**2b**) and $[Pt(SnH_3)_2(CH_3)_2(iPr\text{-}DAB)]$ (**3***) were calculated using the Gaussian 98 programme package (Table 7).

The three types of complexes show different rR spectra (Fig. 3). The main feature of the rR spectrum of $[Pt(I)(CH_3)_3(iPr\text{-}DAB)]$ (**1**) (Fig. 3A) is the presence of only one strong band at 1597 $cm^{-1}$. According to the present DFT calculations and in agreement with results for the related complex $[Ru(I)(CH_3)(CO)_2(iPr\text{-}DAB)]$,[48] this band is assigned to $\nu_s$(CN) of the iPr-DAB ligand. The calculated wavenumber of this vibration of 1647 $cm^{-1}$ is about 3% too high, which is a usual deviation for DFT calculated frequencies using B3LYP potentials and double ζ basis sets. A scaling factor of 0.961 was recommended in the literature.[49] For all complexes, this $\nu_s$(CN) vibration has a CC-stretching motion contribution, similar to that shown for **3*** in Fig. 4. The spectrum shows a few other, much weaker, bands. One of them, the 1226 $cm^{-1}$ band (calculated 1283 $cm^{-1}$) is ascribed to an umbrella type deformation of the axial methyl group on the basis of the calculations, while the band at 553 $cm^{-1}$ (calculated 572 $cm^{-1}$) belongs to the symmetric $C_{eq}$–Pt–$C_{eq}$ stretching motion.

**Table 7** Calculated (unscaled) and observed ($cm^{-1}$) resonance Raman bands[a]

| Complex | Raman bands/$cm^{-1}$ | | | | | |
|---|---|---|---|---|---|---|
| | | | $\nu_s(CN)$ | $\delta_s(CH_3)_{ax}$ | | $\nu_s(PtC)_{eq}$ |
| [Pt(I)$(CH_3)_3$(iPr-DAB)] (**1**, calc) | | | 1647 | 1283 | 584 | 572 |
| [Pt(I)$(CH_3)_3$(iPr-DAB)] (**1**) | | | 1597 | 1226 | 572 | 553 |
| | $\nu_s(CN) + \delta_s(CH_3)_{ax}$ | $2 \times \delta_s(CH_3)_{ax}$ | $\nu_s(CN)$ | $\delta_s(CH_3)_{ax}$ | $\nu_s(PtC)_{eq}$ | $\nu_s(PtC)_{ax}$ |
| [Pt$(CH_3)_4$(iPr-DAB)] (**2a**, calc) | | | 1592 | 1221 | 574 | 497 |
| [Pt$(CH_3)_4$(iPr-DAB)] (**2a**) | 2731 | 2320 | 1564 | 1175 | 517 | 469 |
| [Pt$(CD_3)_4$(iPr-DAB)] (**2b**, calc) | | | 1585 | 931 | | 454 |
| [Pt$(CD_3)_4$(iPr-DAB)] (**2b**) | 2478 | 1802 | 1567 | 894 | n.o.[b] | n.o.[b] |
| [Pt$(CH_3)_4$(tBu-DAB)] (**2c**) | 2759 | 2325 | 1585 | 1173 | 525 | 477 |
| [Pt$(CH_3)_4$(cHx-DAB)] (**2d**) | 2720 | 2334 | 1548 | 1171 | 518 | 472 |
| [Pt$(CH_3)_4$(Xyl-DAB)] (**2e**) | | | [c] | 1159 | | |
| [Pt$(CH_3)_4$(tBu-Pyca)] (**2f**) | | | [d] | 1177 | 583 | 520 |
| [Pt$(CH_3)_4$(tmphen)] (**2g**) | | | [e] | 1173 | [f] | |
| | | | $\nu_s(CN)$ | $\delta_s(CH)/\nu_s(CN)$ | $\delta_s(DAB)$ | $\delta_s(DAB)$ |
| [Pt$(SnH_3)_2(CH_3)_2$(iPr-DAB)](**3***, calc) | | | 1540 | 1354 | 963 | 876 |
| [Pt$(SnPh_3)_2(CH_3)_2$(iPr-DAB)] (**3**) | | | 1475 | 1293 | 948 | 834 |

[a] In the assignments the major contribution is mentioned, see text for more details. [b] Not observed. [c] $\nu_s(CN)$ and ring stretching motions observed at 1607, 1554, 1504, 1302 $cm^{-1}$. [d] $\nu_s(CN)$ and ring stretching motions observed at 1625, 1564, 1482, 1302, 1263, 1248, 1157, 1077, 1025 $cm^{-1}$. [e] $\nu_s(CN)$ and ring stretching motions observed at 1648, 1585, 1521, 1441, 1385, 1313, 1246 $cm^{-1}$. [f] Metal–ligand stretching and ligand deformation vibrations observed at 798, 746, 640, 581, 533, 511, 465 $cm^{-1}$.

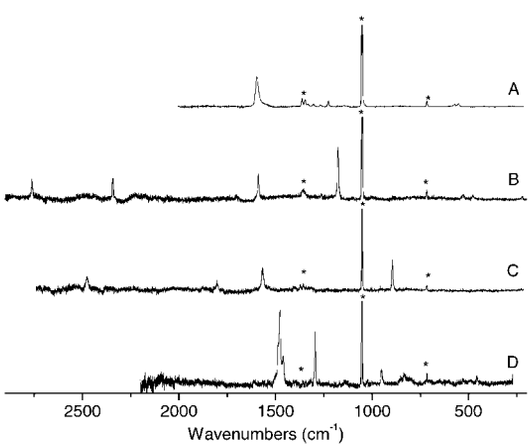


**Fig. 3** Resonance Raman spectra obtained by excitation into the lowest-energy absorption band of (A) [Pt(I)$(CH_3)_3$(iPr-DAB)] (**1**) ($\lambda_{exc}$ = 457.9 nm), (B) [Pt$(CH_3)_4$(iPr-DAB] (**2a**) ($\lambda_{exc}$ = 488.0 nm), (C) [Pt$(CD_3)_4$(iPr-DAB)] (**2b**) and (D) [Pt$(SnPh_3)_2(CH_3)_2$(iPr-DAB)] (**3**) ($\lambda_{exc}$ = 595.6 nm) in $KNO_3$. Asterisks denote $NO_3^-$ bands.

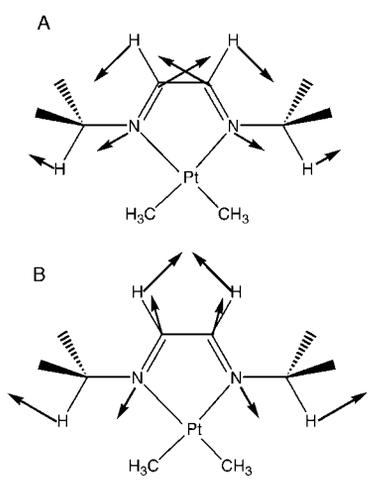


**Fig. 4** Schematic pictures of the displacements (calculated for the model complex **3***) that belong to the two most resonance enhanced vibrations of [Pt$(SnPh_3)_2(CH_3)_2$(iPr-DAB)] (**3**), *viz.* $\nu_s(CN)$ (A) and $\delta_s(CH)$ (B). The $SnH_3$ axial ligands were omitted for clarity; see text for details.

The absence of a rR effect for the Pt–I stretching vibration is in contrast to the rR spectra for [Re(I)$(CO)_3$(iPr-DAB)], which show resonance enhancement of $\nu$(Re–I) on excitation into its XLCT transition.[50] However, if the orbital from which the electronic transition originates has only a minor contribution from the metal, the Pt–I bond need not be affected and $\nu$(Pt–I) may not be resonance enhanced. No bands are observed above 2000 $cm^{-1}$. These results are in agreement with the XLCT (X = I) character of the electronic transition.

The rR spectra of [Pt$(CH_3)_4$(R-DAB)] (**2a**–**d**) show the same $\nu_s(CN)$ vibration at 1548–1585 $cm^{-1}$, the calculated value (1592 $cm^{-1}$) being again a few percent too high. The lower frequency of this vibration compared to that of **1**, is due to π-backbonding to the R-DAB ligand both by d–π* and σ–π* interactions. Since π*(R-DAB) is antibonding with respect to the CN bonds, occupation of this orbital in the ground state leads to a weakening of that bond and a decrease of its frequency. A further increase of the π-backbonding is observed in the rR spectra of **3** ($\nu_s(CN)$ = 1475 $cm^{-1}$, *vide infra*), in agreement with the MO calculations (*vide supra*).

However, whereas $\nu_s(CN)$ is the only vibration that gives rise to a strong Raman band in the case of **1**, an even stronger band is observed at 894 $cm^{-1}$ for **2b** and at *ca.* 1170 $cm^{-1}$ for **2a**, **2c** and **2d**. This is a clear indication that the character of the lowest-energy electronic transition is different for complexes **1** and **2**. A similar band has been observed before, although much weaker, in the rR spectra of [Re(R)$(CO)_3$(dmb)] (R = $CH_3$, $CD_3$; dmb = 4,4′-dimethyl-2,2′-bipyridine) and then shifted from 1166 to 898 $cm^{-1}$ upon deuteration of the methyl ligand.[51] Based on the calculations and the observed frequency shift upon deuteration, it is assigned to a symmetric umbrella-like vibration of the axial methyl groups, $\delta_s(CH_3/CD_3)$. Its overtone is observed at *ca.* 2330 $cm^{-1}$ for the [Pt$(CH_3)_4$(R-DAB)] complexes and at 1802 $cm^{-1}$ for the $CD_3$ complex **2b**, while the combination band of $\nu_s(CN)$ and $\delta_s(CH_3/CD_3)$ is observed at 2720–2770 $cm^{-1}$ and 2478 $cm^{-1}$ for the two types of complexes, respectively. The observation of this strong rR effect for $\delta_s(CH_3/CD_3)$ is in line with the SBLCT character of the electronic transition, since such a transition lowers the electron density in the Pt–$CH_3$ bonds, which in turn causes a change in the $CH_3$ angles. The large change in these angles is demonstrated both by the high Raman intensity of this vibration and by the observation of its overtone. Such overtones are only resonance enhanced if the potential energy curve of the excited state is strongly dis-

**Table 8** Absorption and emission data of the complexes in a 2-MeTHF glass at 90 K

| | Compound | $\lambda_{abs}$/nm | $\lambda_{em}$/nm | $\Delta E_{abs-em}$/cm$^{-1}$ | $\tau/10^2$ ns |
|---|---|---|---|---|---|
| **1** | $[Pt(I)(CH_3)_3(iPr\text{-}DAB)]$ | 373 | 550 | 8628 | 69 |
| **2a** | $[Pt(CH_3)_4(iPr\text{-}DAB)]$ | 464 | 775 | 8464 | 0.25 |
| **2c** | $[Pt(CH_3)_4(tBu\text{-}DAB)]$ | 464 | 750 | 8218 | 0.35 |
| **2d** | $[Pt(CH_3)_4(cHx\text{-}DAB)]$ | 457 | 775 | 8979 | 0.44 |
| **2e** | $[Pt(CH_3)_4(Xyl\text{-}DAB)]$ | 535 | 805 | 6269 | 0.19 |
| **2f** | $[Pt(CH_3)_4(tBu\text{-}Pyca)]$ | 449 | 694 | 7850 | 1.8 |
| **2g** | $[Pt(CH_3)_4(tmphen)]$ | 416 | 600 | 7371 | 93 |
| **3** | $[Pt(SnPh_3)_2(CH_3)_2(iPr\text{-}DAB)]$ | 615 | 809 | 3899 | 12 |

placed with respect to that of the ground state along the normal coordinate of its vibration.[47] The symmetrical $C_{ax}$–Pt–$C_{ax}$ stretching vibration is also affected by the SBLCT transition and is observed as a weak band at about 470 cm$^{-1}$. The band at *ca.* 520 cm$^{-1}$ is ascribed to the symmetrical $C_{eq}$–Pt–$C_{eq}$ stretching vibration on the basis of the calculations. The rR spectra of the other $[Pt(CH_3)_4(\alpha\text{-diimine})]$ complexes (**2e**–**g**) are more complicated since in addition to $\delta_s(CH_3)$, many ring-stretching motions of the ligands are resonantly enhanced. For $[Pt(CH_3)_4(tmphen)]$ (**2g**), a number of metal–ligand stretching and ligand deformation modes are observed additionally between 465 and 798 cm$^{-1}$.

The rR spectrum of $[Pt(SnPh_3)_2(CH_3)_2(iPr\text{-}DAB)]$ (**3**) shows, apart from $\nu_s$(CN) (at 1475 cm$^{-1}$), a strong band at 1293 cm$^{-1}$. According to the vibrational calculations of $[Pt(SnH_3)_2(CH_3)_2(iPr\text{-}DAB)]$ (**3***), this band, calculated at 1354 cm$^{-1}$, belongs to an in plane $\delta_s$(imine CH) mode, combined with $\nu_s$(CN) and with a contribution from $\nu$(CC) (see Fig. 4). Recently measured rR spectra of the isoelectronic complex $[Os(SnPh_3)_2(CO)_2(iPr\text{-}DAB)]$ show the same band at 1272 cm$^{-1}$.[16,19] The 948 and 834 cm$^{-1}$ bands correspond to ligand deformation bands. They were also found for the $[M(SnPh_3)_2(CO)_2(iPr\text{-}DAB)]$ (M = Ru, Os) complexes. These bands always show strong enhancement of Raman intensity whenever the frontier orbitals are more delocalised over the complex, either through d–π* interaction or through σ–π* interaction. As noted before, the σ–π* interaction in **3** is weaker than in the above mentioned Ru and Os complexes, and these ligand deformation modes are indeed much more resonance enhanced for the latter complexes.[16,19]

### Low-temperature emission spectra

Absorption and time-resolved emission spectra were recorded for all complexes in a 2-MeTHF glass at 90 K, under which conditions they are virtually photostable. The absorption bands are blue-shifted by about 20 nm compared to room temperature, due to the rigidochromic effect.[52] Similar blue shifts are observed in the case of $[M(L_1)(L_2)(CO)_2(\alpha\text{-diimine})]$ (M = Ru, Os; $L_1$, $L_2$ = *e.g.* $CH_3$, $SnPh_3$, $Mn(CO)_5$, $RuCp(CO)_2$, *etc.*).[16–20] Table 8 shows the maxima of the lowest-energy absorption and of the emission, as well as the emission lifetimes.

First of all, $[Pt(I)(CH_3)_3(iPr\text{-}DAB)]$ (**1**) emits in a glass at 90 K from its XLCT state with a lifetime of 6.9 μs, which is quite normal for charge transfer states at low temperatures. It is slightly longer than the XLCT emission lifetime of the related complex $[Ru(I)(CH_3)(CO)_2(iPr\text{-}DAB)]$ (1.8 μs),[53] due to its higher emission energy.

Although $[Pt(CH_3)_4(bpy)]$ was reported to be non-emissive even in a glass,[5] the $[Pt(CH_3)_4(\alpha\text{-diimine})]$ complexes were found by us to emit weakly. Reproducible lifetimes of a few tens of nanoseconds were measured for the R-DAB complexes **2a**–**2e**, while a lifetime of 180 ns was found for the tBu-Pyca complex **2f** and 9.3 μs for the tmphen complex **2g**. The reason for this increase in lifetime is twofold. First of all, the emissions of the $[Pt(CH_3)_4(\alpha\text{-diimine})]$ complexes containing (semi)-aromatic α-diimine ligands are at higher energies than those of their R-DAB counterparts. Due to this larger energy gap, non-radiative decay processes are slowed down,[54] and since the excited state mainly decays through these processes ($k_{nr} \gg k_r$), the excited state lifetime increases. The other reason is that the complexes of the (semi)aromatic ligands are less distorted in their excited states. A rough estimate of the distortion of a complex in its excited state with respect to its ground state is the apparent Stokes shift, *i.e.* the energy difference between the absorption and emission maxima. Again, decreasing the distortion in the excited state limits the vibrational overlap between ground and excited states and thus slows down non-radiative decay processes.[55,56] The emission lifetimes of the $[Pt(CH_3)_4(\alpha\text{-diimine})]$ complexes are quite short compared to those of other complexes with a lower SBLCT state, such as $[Ru(L_1)(L_2)(CO)_2(\alpha\text{-diimine})]$, where $L_1$ and $L_2$ are alkyl groups or metal fragments.[16,18–20] For instance, the complex $[Ru(CH_3)(SnPh_3)(CO)_2(iPr\text{-}DAB)]$ emits at 715 nm with a lifetime of 32 μs in a glass at 80 K, whereas **2a** emits at 775 nm with a lifetime of 25 ns under these circumstances. This difference is too large to be ascribed to an energy-gap-law effect, but may be due to two other factors. First of all, all complexes except those containing aromatic DAB ligands, were not completely photostable under the measurement conditions, as could be seen from a change of colour upon prolonged irradiation. In view of this slight photolability, great care was taken to ensure that the observed emissions were not due to artifacts. Secondly, the Pt complexes are more distorted in their SBLCT states than the Ru ones, which is evident from a comparison of their Stokes shifts. This shift is *e.g.* 8464cm$^{-1}$ for **2a** but only 5974 cm$^{-1}$ for $[Ru(CH_3)(SnPh_3)(CO)_2(iPr\text{-}DAB)]$.[16]

The low temperature absorption and emission spectra of $[Pt(SnPh_3)_2(CH_3)_2(iPr\text{-}DAB)]$ (**3**) are shown in Fig. 5. This complex is not only completely photostable in a glass, but also much less distorted in its excited state ($\Delta E_{abs-em}$ = 3899 cm$^{-1}$) than the complexes **2**. This causes a dramatic increase in the low-temperature excited state lifetime from 25 ns to 1.2 μs going from **2a** to **3**, although the emission energy of **3** (809 nm) is lower than that of **2a** (775 nm). The emission of **3** (1.2 μs) is somewhat shorter lived than the XLCT emission of **1** (6.9 μs) but the latter complex emits at much higher energy (550 compared to 809 nm). Such long emission lifetimes as observed for **3** are a general feature of these metal–metal bonded complexes with a lowest SBLCT excited state. For comparison, the isoelectronic complex $[Os(SnPh_3)_2(CO)_2(iPr\text{-}DAB)]$ has a longer excited state lifetime of 32 μs, but it emits at higher energy (655 nm compared to 809 nm for **3**).[19]

## Conclusions

The results discussed in this paper clearly show how strongly the character of the electronic transitions and the emission spectra are influenced by variation of the axial co-ligands in these octahedral Pt(IV) complexes. Both the DFT calculations and resonance Raman spectra established the SBLCT character of the lowest allowed electronic transition of the $[PtMe_4(\alpha\text{-diimine})]$ complexes and $[Pt(SnPh_3)(CH_3)_2(iPr\text{-}DAB)]$.

The excited state properties of the Pt complexes are very similar to those of the corresponding Ru and Os complexes. The series of complexes possessing a lowest-energy SBLCT state now comprise mononuclear complexes, *e.g.* $[Re(R)(CO)_3(\alpha\text{-diimine})]$ (R = alkyl),[12,13] binuclear metal–metal bonded

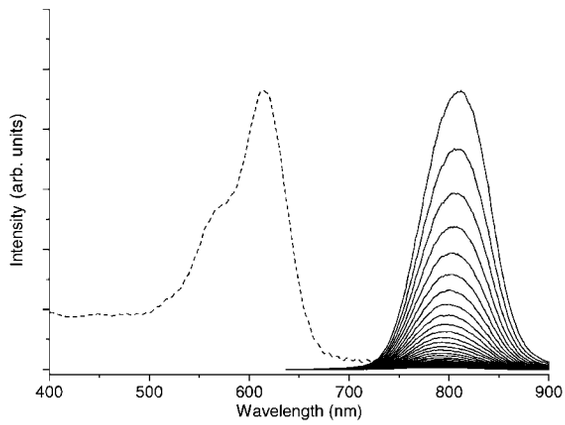


**Fig. 5** Absorption (---) and time-resolved emission (—) spectra of **3** in a 2-MeTHF glass at 90 K. Time delay between the emission spectra is 250 ns.

complexes, *e.g.* $[Re(L)(CO)_3(\alpha\text{-diimine})]$ (L = metal fragment),[14] or $[Ru(CH_3)(SnPh_3)(CO)_2(iPr\text{-}DAB)]$,[16] as well as trinuclear metal–metal bonded complexes, with a linear configuration, *e.g.* $[M(L_1)(L_2)(CO)_2(\alpha\text{-diimine})]$ (M = Ru, Os; $L_1$, $L_2$ = *e.g.* $SnPh_3$, $Mn(CO)_5$, $RuCp(CO)_2$, *etc.*),[16–20] or a triangular configuration, *e.g.* $[Os_3(CO)_{10}(\alpha\text{-diimine})]$.[57,58]

## Acknowledgements

Miss A.L. Vermeer is kindly thanked for experimental contributions. Mr F.W. Vergeer is thanked for recording the $^{13}C$ NMR spectrum of **3**. This work has been undertaken as a part of the European collaborative COST project (D14/0001/99).

## References

1 D. E. Clegg, J. R. Hall and G. A. Swile, *J. Organomet. Chem.*, 1972, **38**, 403.
2 Y. Kondo, M. Ishikawa and K. Ishihara, *Inorg. Chim. Acta*, 1996, **241**, 81.
3 G. S. Hill, G. P. A. Yap and R. J. Puddephatt, *Organometallics*, 1999, **18**, 1408.
4 J. E. Hux and R. J. Puddephatt, *J. Organomet. Chem.*, 1988, **346**, C31.
5 J. E. Hux and R. J. Puddephatt, *J. Organomet. Chem.*, 1992, **437**, 251.
6 W. Kaim, A. Klein, S. Hasenzahl, H. Stoll, S. Záliš and J. Fiedler, *Organometallics*, 1998, **17**, 237.
7 A. Klein, S. Hasenzahl and W. Kaim, *J. Chem. Soc., Perkin Trans. 2*, 1997, 2573.
8 S. Hasenzahl, H.-D. Hausen and W. Kaim, *Chem. Eur. J.*, 1995, **1**, 95.
9 J. van Slageren, D. M. Martino, C. J. Kleverlaan, A. P. Bussandri, H. van Willigen and D. J. Stufkens, *J. Phys. Chem. A*, 2000, **104**, 5969.
10 D. J. Stufkens and A. Vlček, Jr., *Coord. Chem. Rev.*, 1998, **177**, 127.
11 D. J. Stufkens, M. P. Aarnts, J. Nijhoff, B. D. Rossenaar and A. Vlček, Jr., *Coord. Chem. Rev.*, 1998, **171**, 93.
12 B. D. Rossenaar, M. W. George, F. P. A. Johnson, D. J. Stufkens, J. J. Turner and A. Vlček, Jr., *J. Am. Chem. Soc.*, 1995, **117**, 11582.
13 B. D. Rossenaar, C. J. Kleverlaan, M. C. E. van de Ven, D. J. Stufkens and A. Vlček, Jr., *Chem. Eur. J.*, 1996, **2**, 228.
14 B. D. Rossenaar, E. Lindsay, D. J. Stufkens and A. Vlček, Jr., *Inorg. Chim. Acta*, 1996, **250**, 5.
15 J. C. Luong, R. A. Faltynek and M. S. Wrighton, *J. Am. Chem. Soc.*, 1980, **102**, 7892.
16 M. P. Aarnts, D. J. Stufkens, M. P. Wilms, E. J. Baerends, A. Vlček, Jr., I. P. Clark, M. W. George and J. J. Turner, *Chem. Eur. J.*, 1996, **2**, 1556.
17 M. P. Aarnts, M. P. Wilms, K. Peelen, J. Fraanje, K. Goubitz, F. Hartl, D. J. Stufkens, E. J. Baerends and A. Vlček, Jr., *Inorg. Chem.*, 1996, **35**, 5468.
18 M. P. Aarnts, M. P. Wilms, D. J. Stufkens, E. J. Baerends and A. Vlček, Jr., *Organometallics*, 1997, **16**, 2055.
19 J. van Slageren and D. J. Stufkens, *Inorg. Chem.*, 2001, **40**, 277.
20 J. van Slageren, F. Hartl and D. J. Stufkens, *Eur. J. Inorg. Chem.*, 2000, 847.
21 J. M. Kliegman and R. K. Barnes, *Tetrahedron*, 1970, **26**, 2555.
22 J. D. Scott and R. J. Puddephatt, *Organometallics*, 1986, **5**, 1538.
23 R. van Asselt, E. Rijnberg and C. J. Elsevier, *Organometallics*, 1994, **13**, 706.
24 E. J. Baerends, A. Bérces, C. Bo, P. M. Boerrigter, L. Cavallo, L. Deng, R. M. Dickson, D. E. Ellis, L. Fan, T. H. Fischer, C. Fonseca Guerra, S. J. A. van Gisbergen, J. A. Groeneveld, O. V. Gritsenko, F. E. Harris, P. van den Hoek, H. Jacobsen, G. van Kessel, F. Kootstra, E. van Lenthe, V. P. Osinga, P. H. T. Philipsen, D. Post, C. C. Pye, W. Ravenek, P. Ros, P. R. T. Schipper, G. Schreckenbach, J. G. Snijders, M. Sola, D. Swerhone, G. teVelde, P. Vernooijs, L. Versluis, O. Visser, E. van Wezenbeek, G. Wiesenekker, S. K. Wolff, T. K. Woo, T. Ziegler, ADF 1999.01, Amsterdam, 1999.
25 C. Fonseca Guerra, J. G. Snijders, G. te Velde and E. J. Baerends, *Theor. Chem. Acc.*, 1998, **99**, 391.
26 M. J. Frisch, G. W. Trucks, H. B. Schlegel, G. E. Scuseria, M. A. Robb, J. R. Cheeseman, V. G. Zakrzewski, J. J. A. Montgomery, R. E. Stratmann, J. C. Burant, S. Dapprich, J. M. Millam, A. D. Daniels, K. N. Kudin, M. C. Strain, O. Farkas, J. Tomasi, V. Barone, M. Cossi, R. Cammi, B. Mennucci, C. Pomelli, C. Adamo, S. Clifford, J. Ochterski, G. A. Petersson, P. Y. Ayala, Q. Cui, K. Morokuma, D. K. Malick, A. D. Rabuck, K. Raghavachari, J. B. Foresman, J. Cioslowski, J. V. Ortiz, B. B. Stefanov, G. Liu, A. Liashenko, P. Piskorz, I. Komaromi, R. Gomperts, R. L. Martin, D. J. Fox, T. Keith, M. A. Al-Laham, C. Y. Peng, A. Nanayakkara, C. Gonzalez, M. Challacombe, P. M. W. Gill, B. Johnson, W. Chen, M. W. Wong, J. L. Andres, C. Gonzalez, M. Head-Gordon, E. S. Replogle, J. A. Pople, Gaussian 98, Revision A.7, Pittsburgh, PA, 1998.
27 S. J. A. van Gisbergen, J. G. Snijders and E. J. Baerends, *Comput. Phys. Commun.*, 1999, **118**, 119.
28 D. E. Woon and T. H. Dunning, Jr., *J. Chem. Phys.*, 1993, **98**, 1358.
29 D. Andrae, U. Häussermann, M. Dolg, H. Stoll and H. Preuss, *Theor. Chim. Acta*, 1990, **77**, 123.
30 G. Igel-Mann, H. Stoll and H. Preuss, *Mol. Phys.*, 1988, **65**, 1321.
31 P. J. Stephens, F. J. Devlin, C. F. Cabalowski and M. J. Frisch, *J. Phys. Chem.*, 1994, **98**, 11623.
32 A. D. Becke, *Phys. Rev. A*, 1988, **38**, 3098.
33 J. P. Perdew, *Phys. Rev. A*, 1986, **33**, 8822.
34 M. P. Aarnts, D. J. Stufkens, A. Oskam, J. Fraanje and K. Goubitz, *Inorg. Chim. Acta*, 1997, **256**, 93.
35 M. P. Aarnts, A. Oskam, D. J. Stufkens, J. Fraanje, K. Goubitz, N. Veldman and A. L. Spek, *J. Organomet. Chem.*, 1997, **531**, 191.
36 M. P. Aarnts, F. Hartl, K. Peelen, D. J. Stufkens, C. Amatore and J.-N. Verpeaux, *Organometallics*, 1997, **16**, 4686.
37 M. C. Janzen, H. A. Jenkins, L. M. Rendina, J. J. Vittal and R. J. Puddephatt, *Inorg. Chem.*, 1999, **38**, 2123.
38 A. J. Canty, H. Jin, B. W. Skelton and A. H. White, *Aust. J. Chem.*, 1999, **52**, 417.
39 C. J. Levy and R. J. Puddephatt, *J. Am. Chem. Soc.*, 1997, **119**, 10127.
40 L. M. Rendina and R. J. Puddephatt, *Chem. Rev.*, 1997, **97**, 1735.
41 D. L. Packett, A. Syed and W. C. Trogler, *Organometallics*, 1988, **7**, 159.
42 C. Müller and U. Schubert, *Chem. Ber.*, 1991, **124**, 2181.
43 M. Turki, C. Daniel, S. Záliš, A. Vlček, Jr., J. van Slageren and D. J. Stufkens, *J. Am. Chem. Soc.*, 2001, **123**, 11431.
44 M. P. Wilms, E. J. Baerends, A. Rosa and D. J. Stufkens, *Inorg. Chem.*, 1997, **36**, 1541.
45 G. J. Stor, D. J. Stufkens, P. Vernooijs, E. J. Baerends, J. Fraanje and K. Goubitz, *Inorg. Chem.*, 1995, **34**, 1588.
46 J. van Slageren, A. Klein, S. Záliš and D. J. Stufkens, *Coord. Chem. Rev.*, 2001, **219–221**, 967.
47 R. J. H. Clark and T. J. Dines, *Angew. Chem., Int. Ed. Engl.*, 1986, **25**, 131.
48 C. J. Kleverlaan, D. J. Stufkens, J. Fraanje and K. Goubitz, *Eur. J. Inorg. Chem.*, 1998, 1243.
49 M. W. Wong, *Chem. Phys. Lett.*, 1996, **256**, 391.
50 B. D. Rossenaar, D. J. Stufkens and A. Vlček, Jr., *Inorg. Chem.*, 1996, **35**, 2902.
51 C. J. Kleverlaan and D. J. Stufkens, *Inorg. Chim. Acta*, 1999, **284**, 61.
52 A. J. Lees, *Comments Inorg. Chem.*, 1995, **17**, 319.
53 H. A. Nieuwenhuis, D. J. Stufkens and A. Vlček, Jr., *Inorg. Chem.*, 1995, **34**, 3879.
54 R. Englman and J. Jortner, *Mol. Phys.*, 1970, **18**, 145.
55 J. A. Treadway, B. Loeb, R. Lopez, P. A. Anderson, F. R. Keene and T. J. Meyer, *Inorg. Chem.*, 1996, **35**, 2242.
56 G. F. Strouse, J. R. Schoonover, R. Duesing, S. Boyde, W. E. Jones, Jr. and T. J. Meyer, *Inorg. Chem.*, 1995, **34**, 473.
57 J. Nijhoff, M. J. Bakker, F. Hartl, D. J. Stufkens, W.-F. Fu and R. van Eldik, *Inorg. Chem.*, 1998, **37**, 661.
58 M. J. Bakker, F. Hartl, D. J. Stufkens, O. S. Jina, X.-Z. Sun and M. W. George, *Organometallics*, 2000, **19**, 4310.